Electronic Supplementary Material (ESI) for ChemComm.
This journal is © The Royal Society of Chemistry 2018

Electronic Supplementary Information (ESI)

Efficient Excitons Harvest Route for High-Performance OLEDs Based on Aggregation-Induced Delayed Fluorescence

Ling Yu,[a] Zhongbin Wu,[b] Guohua Xie,[a] Cheng Zhong,[a] Zece Zhu,[a] Dongge Ma*[bc] and Chuluo Yang*[a]

[a]Hubei Collaborative Innovation Center for Advanced Organic Chemical Materials, Hubei Key Lab on Organic and Polymeric Optoelectronic Materials, Department of Chemistry, Wuhan University, Wuhan, 430072, People's Republic of China.
[b]State Key Laboratory of Polymer Physics and Chemistry, Changchun Institute of Applied Chemistry, University of Chinese Academy of Sciences, Changchun, 130022, People's Republic of China.
[c]Institute of Polymer Optoelectronic Materials and Devices, State Key Laboratory of Luminescent Materials and Devices, South China University of Technology, Guangzhou, 510640, People's Republic of China

Corresponding Author

**E-mail: clyang@whu.edu.cn (Chuluo Yang)*

**E-mail: mdg1014@ciac.ac.cn (Dongge Ma)*

1. Experimental section

General Information

The ^{1}H NMR and ^{13}C NMR spectra were recorded on a MERCURY-VX300 and Bruker Advance Ⅲ (400 MHz) spectrometer with $CDCl_3$ as the solvent, respectively. Mass spectra were measured on a ZAB 3F-HF mass spectrophotometer. Elemental analyses were performed on a Vario EL-III microanalyzer. Single-crystal X-ray diffraction data were obtained from a Bruker APEX Ⅱ Smart CCD diffractometer. Thermal gravity analysis (TGA) was performed on a Netzsch STA 449C instrument. Differential scanning calorimetry (DSC) was performed on a NETZSCH DSC 200 PC unit at a heating rate of 20 °C min^{-1} from 25 to 350 °C under argon. The glass transition temperature (T_g) was determined from the second heating scan at a heating rate of 10 °C min^{-1}. UV-vis absorption spectra were recorded on a Shimadzu UV-2700 recording spectrophotometer. Photoluminescence (PL) spectra were recorded on a Hitachi F-4600 fluorescence spectrophotometer. Cyclic voltammetry (CV) was carried out in nitrogen-purged dichloromethane (oxidation scan) at room temperature with a CHI voltammetric analyzer. N-Bu_4PF_6 (0.1 M) was used as the supporting electrolyte. The conventional three-electrode configuration consists of a platinum working electrode, a platinum wire auxiliary electrode, and an Ag wire pseudoreference electrode with ferrocenium-ferrocene (Fc^+/Fc) as the internal standard. Cyclic voltammograms were obtained at a scan rate of 100 mV s^{-1}. The onset potential was determined from the intersection of two tangents drawn at the rising and background current of the cyclicvoltammogram. The PL lifetimes were measured by a single photon counting spectrometer from Edinburgh Instruments (FLS920) with a Picosecond Pulsed UV-LASTER (LASTER377) as the excitation source. The photoluminescence quantum

efficiency was measured using an absolute photoluminescence quantum yield measurement system (C9920-02, Hamamatsu Photonics).

Device fabrication and characterization

The device was grown on clean glass substrates pre-coated with a 180-nm-thick ITO with a sheet resistance of 10 Ω per square. The ITO glass substrates were pre-cleaned carefully and treated by oxygen plasma for 2 min. Then the sample was transferred to the deposition system. For the doped devices, 10 nm MoO_3 was firstly deposited onto the ITO substrate, consecutively followed by TAPC: 20% MoO_3 (50 nm), TAPC (20 nm), emissive layer (20 nm), and Bphen (45 nm). For the non-doped devices, 10 nm MoO_3 was firstly deposited onto the ITO substrate, consecutively followed by TAPC (50 nm), mCP (10 nm), emissive layer (30 nm), and Bphen (45 nm). Finally, a cathode composed of lithium fluoride and aluminum was sequentially deposited onto the sample in the vacuum of 10^{-6} Torr. The current-voltage-brightness characteristic was measured by using a Keithley source measurement units (Keithley 2400 and Keithley 2000) with a calibrated silicon photodiode. The EL spectra were measured by a Spectrascan PR650 spectrophotometer. The EQE was calculated from the luminance and current density.

1. Synthesis of materials

SFDBQPXZ and DFDBQPXZ were prepared by nucleophilic substitution reactions of phenoxazine (PXZ) with the key intermediates 2,3-bis(4-bromophenyl)-6-fluoroquinoxaline (SFDBQ) and 2,3-bis(4-bromophenyl)-6,7-difluoroquinoxaline (DFDBQ) (Scheme S1, ESI†). Their chemical structures were verified by ^{1}H and ^{13}C NMR spectroscopies, elemental analysis, mass spectrometry and X-ray crystallographic analysis.

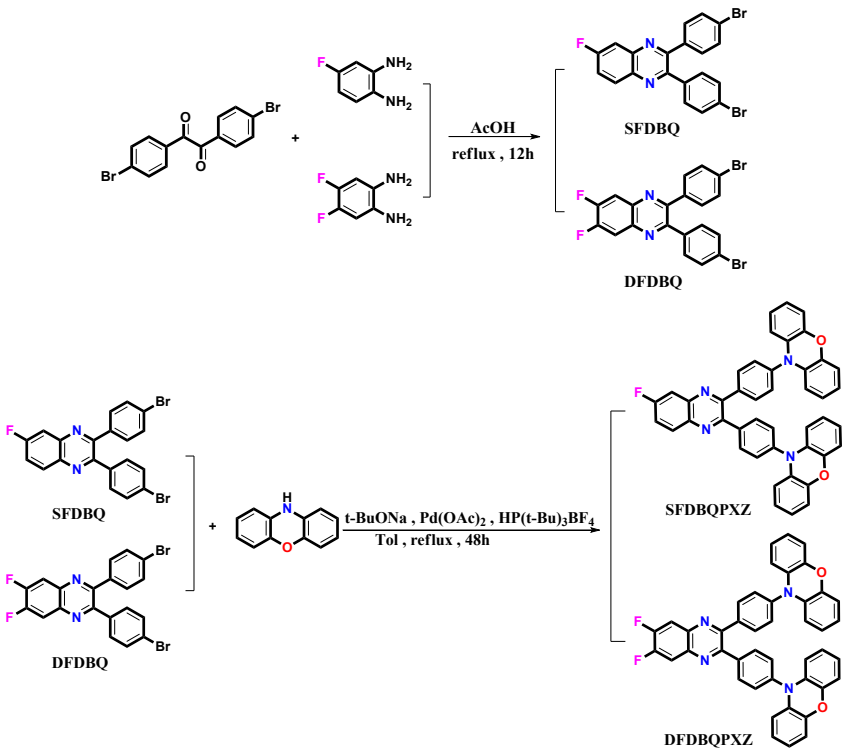

Scheme S1. Synthetic routes of **SFDBQPXZ** and **DFDBQPXZ**.

2,3-bis(4-bromophenyl)-6-fluoroquinoxaline **(SFDBQ)**, 2,3-bis(4-bromophenyl)-6,7-difluoroquinoxaline (**DFDBQ**) were synthesized according to the literature methods.[S1]

10,10'-((6-fluoroquinoxaline-2,3-diyl)bis(4,1-phenylene))bis(10*H*-phenoxazine) (**SFDBQPXZ**): A mixture of **SFDBQ** (1.10 g, 2.40 mmol), phenoxazine (1.01 g, 5.5 mmol), $Pd(OAc)_2$ (20 mg, 0.09

mmol), HP(*t*-Bu)$_3$BF$_4$ (64 mg, 0.22 mmol), *t*-BuONa (0.52 g, 5.42 mmol), and toluene (30 ml) was refluxed under argon for 24 h. After cooled, the mixture was extracted with brine and CH_2Cl_2, and dried over anhydrous Na_2SO_4. After removal of the solvent, the residue was purified by column chromatography on silica gel using dichloromethane/petroleum ether (2:3 by vol.) as the eluent to give a yellow powder (1.46 g, yield: 92%). ^{1}H NMR (300 MHz, $CDCl_3$) δ [ppm]: 8.29-8.24 (m, 1H), 7.89-7.87 (m, 1H), 7.78 (d, *J* = 6.9 Hz, 4H), 7.65 (t, *J* = 8.6 Hz, 1H), 7.40 (d, *J* = 7.8 Hz, 4H), 6.71-6.61 (m, 8H), 6.52 (t, *J* = 7.5 Hz, 4H), 5.95 (d, *J* = 7.5 Hz, 4H). ^{13}C NMR (100 MHz, $CDCl_3$) δ [ppm]: 164.52, 162.01, 153.40, 152.02, 151.98, 143.92, 142.26, 142.13, 139.96 (d, *J* = 16.0 Hz), 138.69 (t, *J* = 6.0 Hz), 133.86, 132.62 (d, *J* = 4.0 Hz), 131.33 (t, *J* = 26.5 Hz), 123.43, 121.34 (t, *J* = 31 Hz), 115.59, 112.94(t, *J* = 19.5 Hz). MS (EI): *m/z* 663 [M$^+$]. EA (%) for $C_{44}H_{27}FN_4O_2$: C 79.74, H 4.11, N 8.45; found: C 79.65, H 4.16, N 8.34. (CCDC: 1555294)

10,10'-((6,7-difluoroquinoxaline-2,3-diyl)bis(4,1-phenylene))bis(10*H*-phenoxazine) (**DFDBQPXZ**): It was prepared using the key intermediate **DFDBQ** with the same manner as above described, and **DFDBQPXZ** shows a yellow powder (1.60 g, yield: 93%). ^{1}H NMR (300 MHz, $CDCl_3$) δ [ppm]: 8.00 (t, *J* = 9.3 Hz, 2H), 7.77 (d, *J* = 8.4 Hz, 4H), 7.40 (d, *J* = 8.1 Hz, 4H), 6.71-6.61 (m, 8H), 6.52 (t, *J* = 7.4 Hz, 4H), 5.94 (d, *J* = 8.1 Hz, 4H). ^{13}C NMR (100 MHz, $CDCl_3$) δ [ppm]: 154.23 (d, *J* = 18.0 Hz), 152.84, 151.65 (d, *J* = 18.0 Hz), 143.93, 140.10, 138.77 (t, *J* = 6.0 Hz), 138.44, 133.81, 132.59, 131.06, 123.43, 121.72, 115.61, 115.10-114.91 (m), 113.12. MS (EI): *m/z* 681 [M$^+$]. EA (%) for $C_{44}H_{26}F_2N_4O_2$: C 77.64, H 3.85, N 8.23; found: C 77.59, H 3.84, N 8.24. (CCDC: 1555295)

2. Single crystal structures data

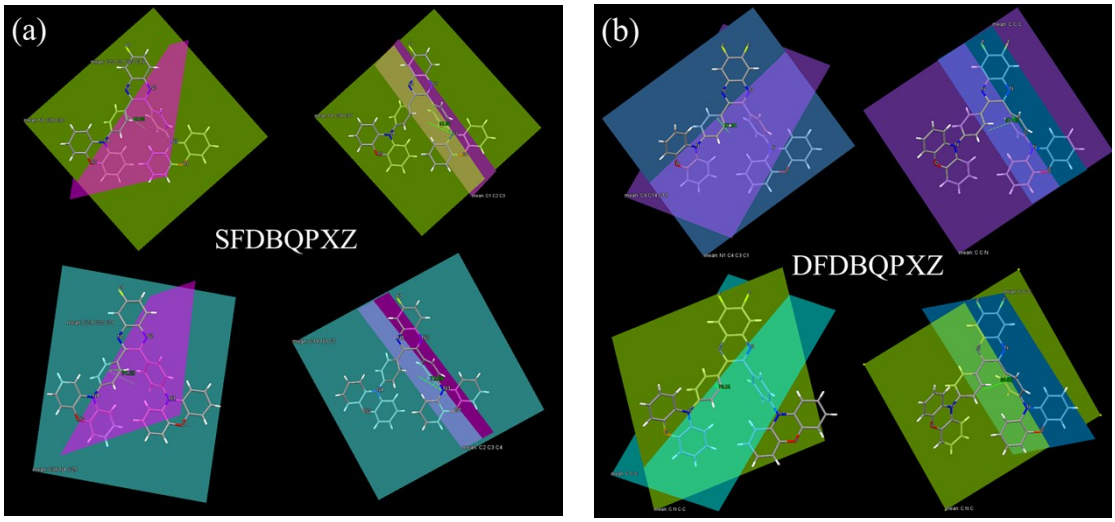

Figure S1. The relevant dihedral angles of single crystal structures: (a) SFDBQPXZ and (b) DFDBQPXZ.

Table S1. Intermolecular distance and short contacts of SFDBQPXZ and DFDBQPXZ in the crystal state

compound	**intermolecular distance (Å) and short contacts**					
	C-H⋯N	**C-H⋯F**	**C-H⋯H-C**	**C-H⋯π**	**C-H⋯O**	**π-π**
SFDBQPXZ	2.664,2.728	2.406	2.331, 2.385	2.745	×	×
DFDBQPXZ	×	2.632	2.397	2.869	2.585	3.395

3. DFT calculation

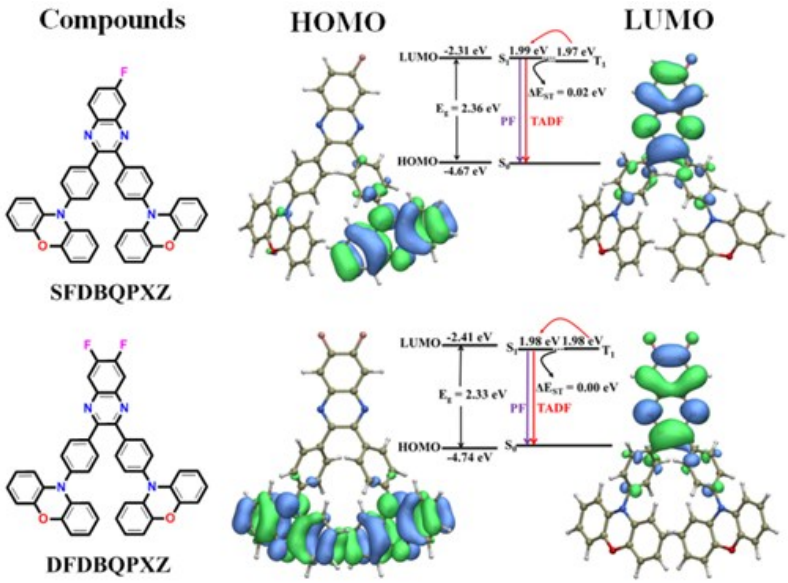

Figure. S2. Molecular structures (left), and the HOMO/LUMO distributions evaluated by using DFT method at B3lyp/6-31g(d) level with Grimme's D3 correction.

Table S2. Values from DFT calculation.

Compound	HOMO [eV]	LUMO [eV]	S_1 [eV]	T_1 [eV]	ΔE_{ST} [eV]	*f*	main configuration[a)]	
SFDBQPXZ	-4.67	-2.31	1.99	1.97	0.02	0.0131	H → L	0.70464
DFDBQPXZ	-4.74	-2.41	1.98	1.98	0.00	0.0002	H → L	0.70455

[a)]H → L represents the HOMO to LUMO transition of the first singlet state.

4. Photophysical, electrochemical and thermal data

Photophysical Property

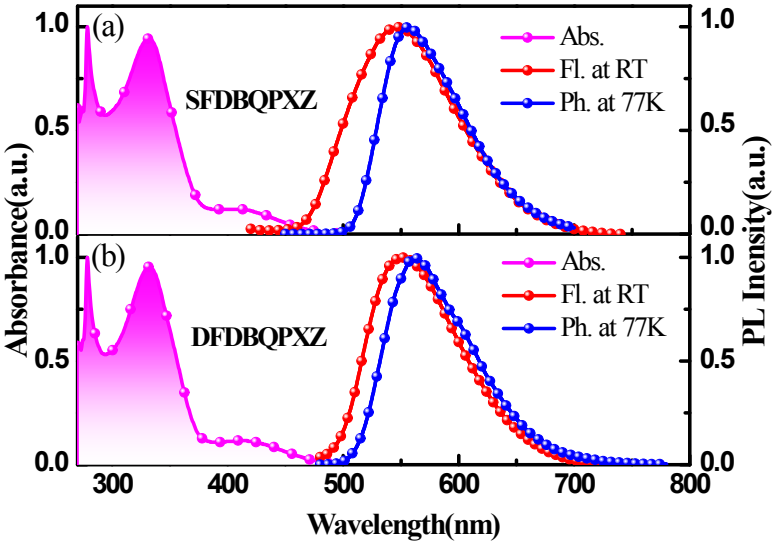

Figure S3. Normalized UV/vis absorption of (a) SFDBQPXZ, and (b) DFDBQPXZ in toluene. Fluorescence and Phosphorescence spectra of these two compounds were measured in film. The pink and the red lines represent UV/vis and fluorescence spectra, respectively, while the blue lines represent phosphorescence spectra.

We measured the UV-vis absorption of the two compounds in toluene and the photoluminescence (PL) properties in film. As shown in Fig. S3 and Table S3 (ESI†), the UV-vis spectra of SFDBQPXZ and DFDBQPXZ exhibit analogical absorption maximum at 414 and 415 nm, respectively, depending on ICT process from the PXZ units to the electron-acceptor core. The neat films of SFDBQPXZ and DFDBQPXZ reveal broad and structureless fluorescence and phosphorescence emission patterns (Fig. S3a and S3b, ESI†). With the increased numbers of fluorine atom, the PL spectra are slightly bathochromic shift. The diminutive experimental ΔE_{ST} values match well with the theoretical calculations and such small ΔE_{ST} can be ultimately utilized for the up-conversion process of the triplet excitons in fluorescent OLEDs. The electrochemical properties of SFDBQPXZ and DFDBQPXZ were probed by cyclic voltammetry (CV), as shown in Fig. S4 (ESI†), respectively.

The similar HOMO/LUMO values reflect the weak influence of the electronic properties when using the fluorine substituent. More details are disclosed in Fig. S5 and Table S3 (ESI†).

Electrochemical Property

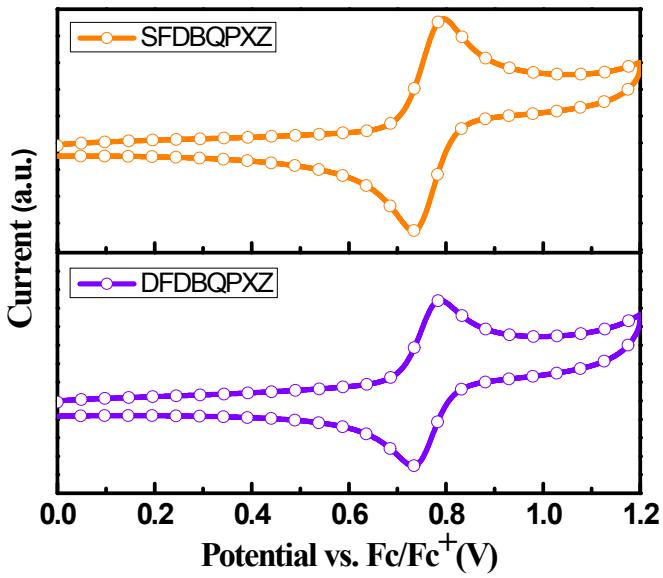

Figure S4. Cyclic voltammogram of SFDBQPXZ and DFDBQPXZ in CH_2Cl_2 for oxidation scan.

Thermal Property

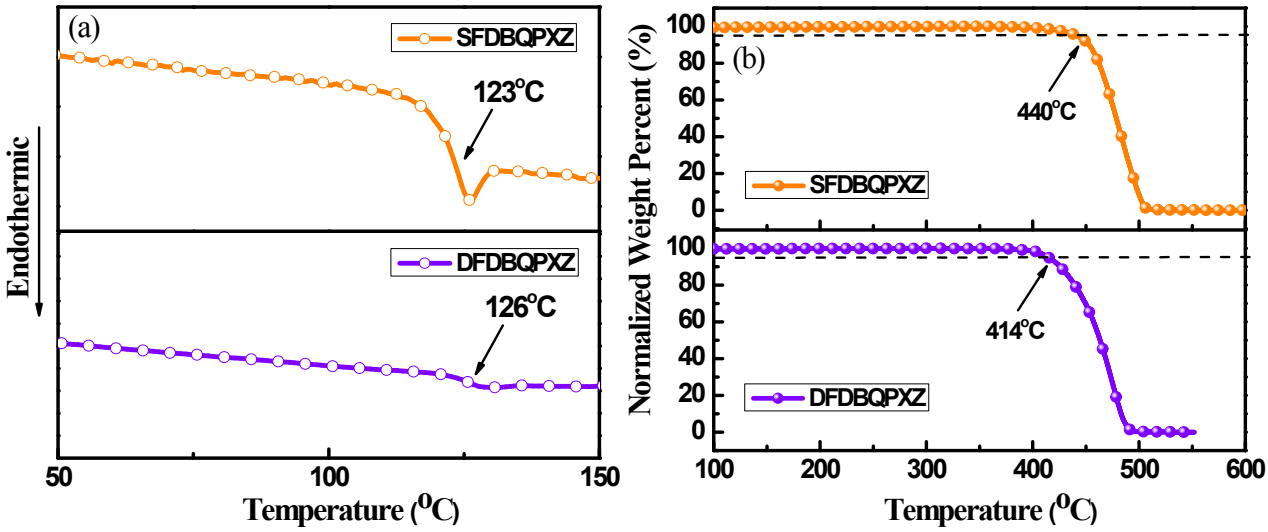

Figure S5. (a) Differential scanning calorimetry (DSC) curves and (b) thermal gravity analysis (TGA) curves of SFDBQPXZ and DFDBQPXZ.

Table S3.Thermal, photophysical, and electrochemical data of the compounds.

Compound	T_d[a)]/T_g[b)] [°C]	λ_{abs}[c)] [nm]	Φ_{PL}[d)] [%]	$\lambda_{Fl,max}$[e)] [nm]	$\lambda_{Ph,max}$[e)] [nm]	E_S/E_T [eV]	ΔE_{ST}[f)] [eV]	ΔE_g[g)] [eV]	HOMO[h)]/LUMO[i)] [eV]
SFDBQPXZ	440/123	331/414	13.8(23.1)/14.4	546	556	2.27/2.23	0.04	2.60	-5.12/-2.52
DFDBQPXZ	415/126	332/415	11.2(21.3)/14.1	551	561	2.25/2.21	0.04	2.58	-5.11/-2.53

[a)]Obtained by TGA. [b)]Obtained by DSC. [c)]Measured in toluene at room tempurature. [d)]Absolute quantum yield in toluene and hexane and the value in bracket represents PLQY after the deoxygenation in toluene. [e)]Measured in film at room temperature and 77 K, respectively. [f)]ΔE_{ST}= E_S- E_T. [g)]Calculated from the absorption edge of the UV/Vis spectrum. [h)]Determined from the onset of the oxidation potential. [i)]Deduced from HOMO and ΔE_g.

AIE Property

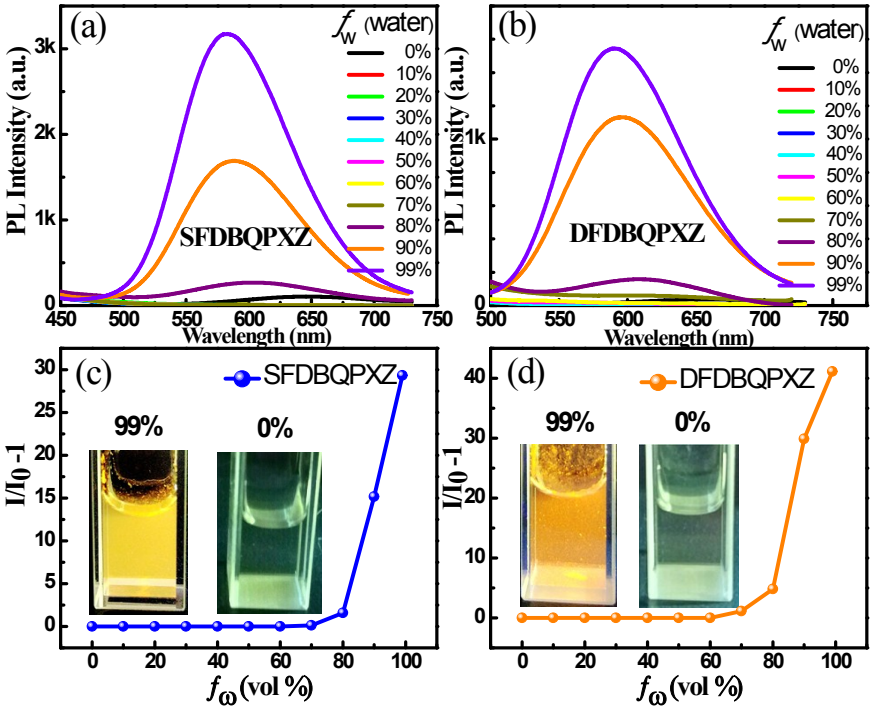

Figure. S6. PL spectra of (a) SFDBQPXZ and (b) DFDBQPXZ in THF/water mixture with different water fractions (f_w). (c-d) Plot of (I/I_0 - 1) values versus water fractions in THF/water mixtures of SFDBQPXZ and DFDBQPXZ. I_0 is the PL intensity in pure THF solution. Inset: photos of SFDBQPXZ and DFDBQPXZ in THF/water mixtures (f_w = 0 and 99%), taken under the illumination of a UV lamp.

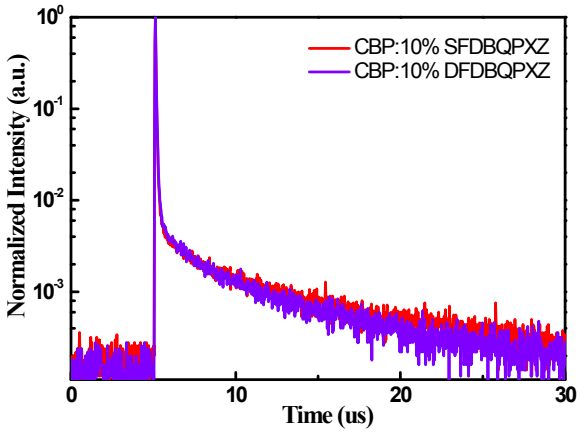

Figure S7. Transient PL decay of CBP:10% TADF in film after the deoxygenation at room temperature.

Table S4. The lifetimes, quantum efficiencies and rate constants of CBP: 10% TADF in film.

TADF Compounds	τ_F [ns]	τ_d [μs]	Φ_{PL} [%]	Φ_{PF}[a)] [%]	Φ_{DF}[a)] [%]	k_P[b)] [s^{-1}]	k_d[b)] [s^{-1}]	k_r^S [c)] [s^{-1}]	k_{ISC}[d)] [s^{-1}]	k_{RISC}[d)] [s^{-1}]
SFDBQPXZ	36	1.5	99.6	61.8	37.8	2.8×10^7	6.7×10^5	1.7×10^7	1.1×10^7	1.0×10^6
DFDBQPXZ	41	2.0	88.3	59.2	29.1	2.4×10^7	5.0×10^5	1.4×10^7	1.0×10^7	5.9×10^5

[a)]The prompt (PF) and delayed (DF) fluorescence quantum yield, respectively. [b)]The rate constants for prompt and delayed fluorescence, respectively. [c)]k_r^S represents the radiative decay rate constants from S_1 to S_0 transition. [d)]The rate constants of intersystem crossing (ISC) and reverse intersystem crossing (RISC) between the S_1 and T_1 states, respectively.

Table S5. The lifetimes, quantum efficiencies and rate constants of TADF in pristine films.

TADF Compounds	τ_F [ns]	τ_d [μs]	Φ_{PL} [%]	Φ_{PF}[a)] [%]	Φ_{DF}[a)] [%]	k_P[b)] [s^{-1}]	k_d[b)] [s^{-1}]	k_r^S[c)] [s^{-1}]	k_{ISC}[d)] [s^{-1}]	k_{RISC}[d)] [s^{-1}]
SFDBQPXZ	57	3.4	43.4	17.4	26.0	1.8×10^7	2.9×10^5	3.1×10^6	1.5×10^7	5.2×10^5
DFDBQPXZ	68	3.3	33.2	14.4	18.8	1.5×10^7	3.0×10^5	2.1×10^6	1.3×10^7	4.5×10^5

[a)]The prompt (PF) and delayed (DF) fluorescence quantum yield, respectively. [b)]The rate constants for prompt and delayed fluorescence, respectively. [c)]k_r^S represents the radiative decay rate constants from S_1 to S_0 transition. [d)]The rate constants of intersystem crossing (ISC) and reverse intersystem crossing (RISC) between the S_1 and T_1 states, respectively.

5. Device performance

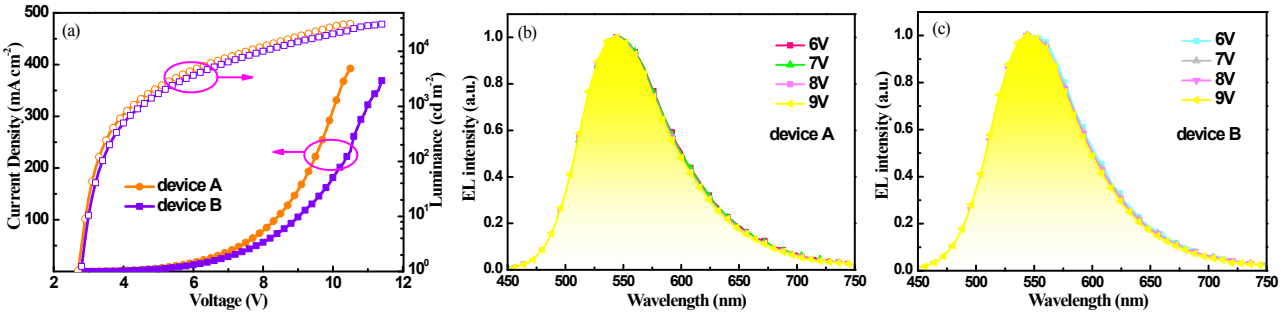

Figure S8. (a) Current density-voltage-brightness characteristics of the doped devices (A and B). (b-c) EL spectra of the doped devices (A and B) measured at different voltages, respectively.

The vacuum-deposited OLEDs were initially fabricated containing SFDBQPXZ (the device A) and DFDBQPXZ (the device B) as the dopants, respectively. The doped device were constructed with the following configuration: ITO/MoO_3 (10 nm)/TAPC: MoO_3 (20%, 50 nm)/TAPC (20 nm)/CBP: TADF (10%, 20 nm)/Bphen (45 nm)/LiF (1 nm)/Al, where 1,1-bis[4-[*N,N*-di(p-tolyl)-amino]phenyl]cyclohexane (TAPC) and 4,7-Diphenyl-1,10-phenanthroline (Bphen) were introduced as the hole- and electron-transporting materials, respectively. To improve the hole-injection efficiency, additional 20% MoO_3 was mixed into the hole-transporting layer. The key device performances of the two devices are displayed in **Fig.3**, S8 (ESI†) and **Table 1**.

The best device performances obtained by the device A, which is well consistent with our assumption and prediction according to the theoretical calculations, are ascribed to the congenital superiority of SFDBQPXZ combining both AIE and TADF properties: (1) a fluorine-substituted asymmetric structure to accelerate large RIR and ensure high quantum efficiency; (2) a quite small ΔE_{ST} to maximize the utilization of the triplet excitons through up-conversion process, realizing a high k_{RISC} (1.0×10^6 s^{-1}); (3) a short DF lifetime to hinder triplet-exciton-involved quenching and to ease the efficiency roll-off.

Table S6. Comparison of the device performance of SFDBQPXZ, DFDBQPXZ and representative TADF/AIE OLEDs with similar emissions in literatures.

Device	Property	EQE_{max} [%]	CE_{max} [cd A^{-1}]	PE_{max} [lm W^{-1}]	Peak[a)] [nm]	Performance at 100/1000 cd m^{-2} EQE[%]	CE[cd A^{-1}]	PE[lm W^{-1}]
SFDBQPXZ	**AIE+TADF**	**23.5**	**78.3**	**91.1**	**548**	**17.0/13.0**	**56.7/43.5**	**54.5/32.2**
DFDBQPXZ	**AIE+TADF**	**16.8**	**55.9**	**57.8**	**548**	**16.4/12.4**	**54.5/41.2**	**50.3/28.8**
Spiro-CN[S2]	TADF	4.4	13.5	13.0	～545	N.A.	N.A.	N.A.
TXO-TPA[S3]	TADF	18.5	43.3	47.4	552	＜18.0/＜10.0	＜30.0/＜20.0	＜10.0/＜5.0
PxPmBPX[S4]	TADF	11.3	35.3	N.A.	541	N.A.	N.A.	N.A.
TPA-PRZ$(CN)_2$[S5]	TADF	4.0	N.A.	N.A.	542	＜4.0/＜4.0	N.A.	N.A.
Bis-PXZTRZ[S6]	TADF	9.1	N.A.	N.A.	～552	＜9.0/＜8.0	N.A.	N.A.
PXZDSO_2[S7]	TADF	16.7	49.3	38.5	560	16.3/13.7	N.A.	N.A.
Py56[S8]	TADF	29.2	96.3	105.5	～550	26.5/20.6	88.1/69.1	63.3/34.7
$(MesB)_2$DMTPS[S9]	AIE	2.25	7.4	3.2	540	＜2.0/＜2.0	＜7.0/＜7.0	＜3.2/＜3.2
$(MesB)_2$HPS[S9]	AIE	2.62	8.4	4.1	548	＜2.6/＜2.6	＜8.4/＜8.4	＜4.1/＜4.1
$(MesB)_2$MPPS[S9]	AIE	2.13	6.6	2.4	552	＜2.0/＜2.0	＜6.6/＜6.6	＜2.4/＜2.4
BPA2TPAN[S10]	AIE	3.3	10.5	7.1	551	N.A.	N.A.	N.A.
BNA2TPAN[S10]	AIE	4.2	12.2	8.3	559	N.A.	N.A.	N.A.
DBT-BZ-PXZ[S11]	AIE+TADF	9.2	26.6	27.9	557	-/6.8	＜26/19.6	＜20.0/11.3
DBT-BZ-PTZ[S11]	AIE+TADF	9.7	26.5	29.1	563	-/8.5	＜26/23.5	＜20.0/15.4

[a)]The peak wavelength of EL spectrum. N.A.: not available.

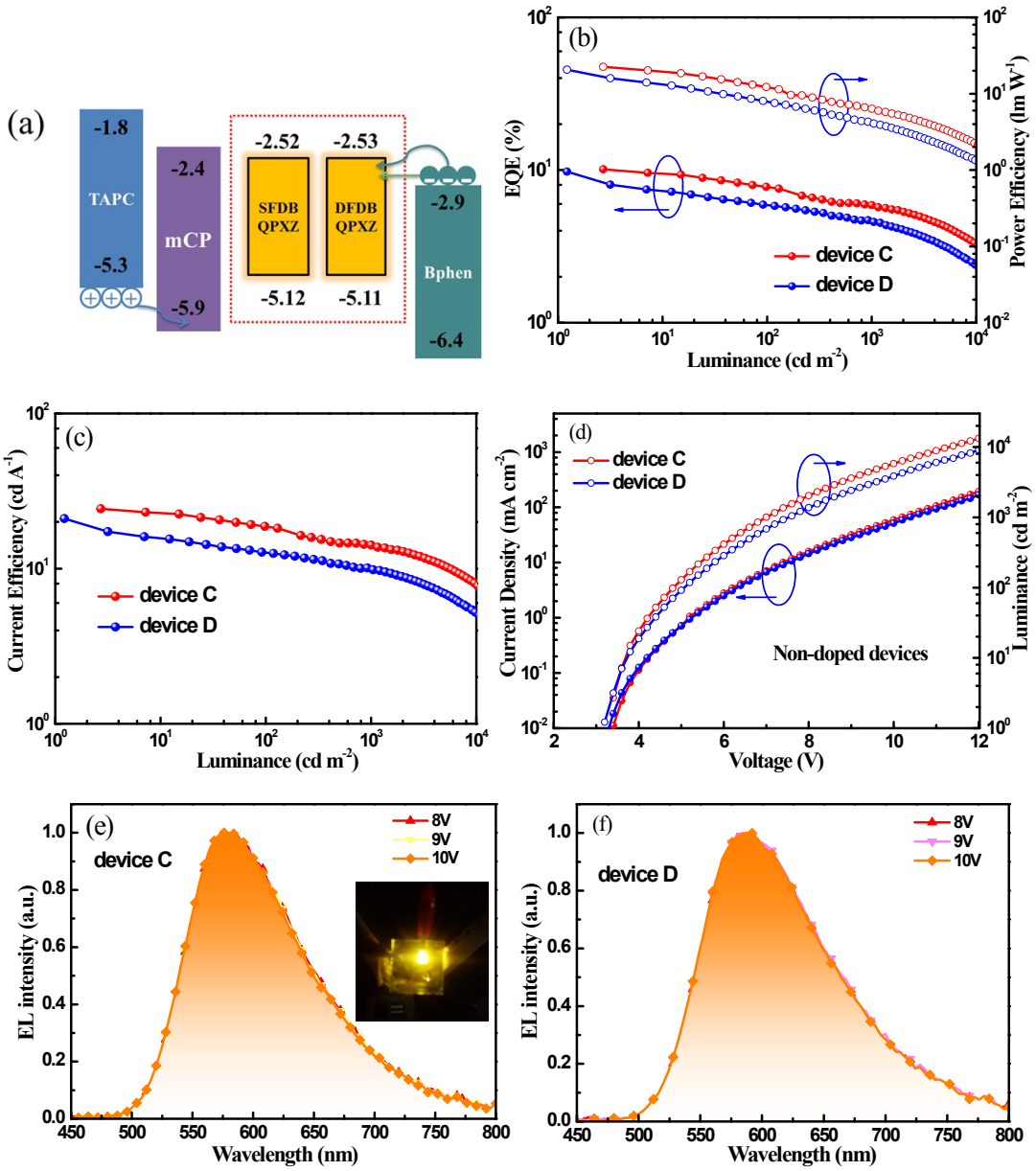

Figure S9. (a) The energy structure of the non-doped devices (C-D). (b) EQE and PE versus luminance curves. (c) Current efficiency versus luminance curves. (d) Current density-voltage-brightness characteristics. (e-f) Normalized EL spectra of the non-doped devices C-D at different voltages. Inset: the image of a working device.

Table S7. The characteristic data of the non-doped devices (C-D).

Device	V_{on} [V]	EQE_{max} [%]	CE_{max} [cd A^{-1}]	PE_{max} [lm W^{-1}]	LE_{max} [cd m^{-2}]	Peak [nm]	Performance at the brightness of 100 and 1000 cd m^{-2}		
							EQE [%]	CE [cd A^{-1}]	PE [lm W^{-1}]
C	**3.4**	**10.1**	**24.3**	**22.5**	**21102**	**584**	**7.7/6.0**	**18.8/14.2**	**12.2/6.3**
D	**3.2**	**9.8**	**21.0**	**20.6**	**16497**	**588**	**5.9/4.7**	**12.9/9.8**	**7.9/4.2**

Table S8. Comparison of the non-doped device performance of SFDBQPXZ, DFDBQPXZ and representative OLEDs with similar emissions in literatures.

Device	property	EQE_{max} [%]	CE_{max} [cd A^{-1}]	PE_{max} [lm W^{-1}]	Peak [nm]	Performance at 100/1000 cd m^{-2}		
						EQE[%]	CE[cd A^{-1}]	PE[lm W^{-1}]
TPA3TPAN[S12]	AIE	2.18	6.16	2.64	580	N.A.	N.A.	N.A.
T_2BT_2[S13]	AIE	2.88	6.81	4.96	590	＜2.8/＜2.8	＜6.0/＜6.0	＜5.0/＜5.0
PCZ-CB-TRZ[S14]	AIE+TADF	11.0	16.7	7.6	586	N.A.	N.A.	N.A.
2PCZ-CB[S14]	AIE+TADF	9.2	19.9	11.2	590	N.A.	N.A.	N.A.
SFDBQPXZ	**AIE+TADF**	**10.1**	**24.3**	**22.5**	**584**	**7.7/6.0**	**18.8/14.2**	**12.2/6.3**
DFDBQPXZ	**AIE+TADF**	**9.8**	**21.0**	**20.6**	**588**	**5.9/4.7**	**12.9/9.8**	**7.9/4.2**

N.A.: not available.

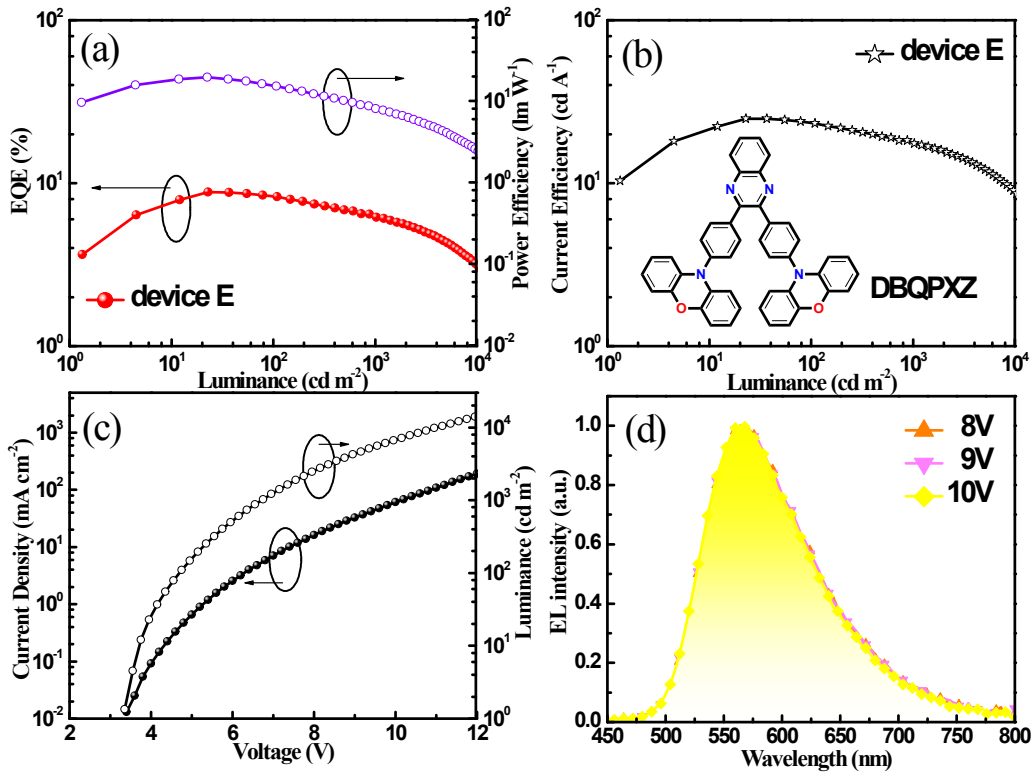

Figure S10. (a) EQE and PE versus luminance curves of the non-doped device E with the non-fluorinated compound of DBQPXZ as emitter; (b) Current efficiency versus luminance curves; (c) Current density-voltage-brightness characteristics; (d) Normalized EL spectra at different voltages.

Table S9. The characteristic data of the non-doped devices (E).

Device	V_{on} [V]	EQE_{max} [%]	CE_{max} [cd A^{-1}]	PE_{max} [lm W^{-1}]	LE_{max} [cd m^{-2}]	Peak (nm)	Performance at the brightness of 100 and 1000 cd m^{-2}		
							EQE [%]	CE [cd A^{-1}]	PE [lm W^{-1}]
E	3.4	8.8	24.9	19.6	20167	564	8.3/6.3	23.5/17.8	15.8/8.3

As a reference, the same non-doped device preparation was used for the non-fluorinated compound DBQPXZ-based device E. The device E exhibits bright yellow emission with an EL peak at 564 nm, accompanied with a maximum luminance of 20167 cd m^{-2}, an EQE_{max} of 8.8%, which is inferior to fluorine-substituted emitters-based devices (Fig. S10 and Table S9, ESI†).

Reference

[S1] S. Jo, J. Kim, J. Noh, D. Kim, G. Jang, N. Lee, E. Lee, T. S. Lee, *Appl. Mater. Interfaces*, 2014, **6**, 22884.

[S2] T. Nakagawa, S. Y. Ku, K. T. Wong, C. Adachi, *Chem. Commun.* 2012, **48**, 9580.

[S3] H. Wang, L. Xie, Q. Peng, L. Meng, Y. Wang, Y. Yi, P. Wang, *Adv. Mater.* 2014, **26**, 5198.

[S4] S. Y. Lee, T. Yasuda, I. S. Park, C. Adachi, *Dalton Trans.* 2015, **44**, 8356.

[S5] K. Kawasumi, T. Wu, T. Zhu, H. S. Chae, T. Van Voorhis, M. A. Baldo, T. M. Swager, *J. Am. Chem. Soc.* 2015, **137**, 11908.

[S6] H. Tanaka, K. Shizu, H. Nakanotani, C. Adachi, *Chem. Mater.* 2013, **25**, 3766.

[S7] G. Xie, X. Li, D. Chen, Z. Wang, X. Cai, D. Chen, Y. Li, K. Liu, Y. Cao, S. J. Su, *Adv. Mater.* 2016, **28**, 181.

[S8] K.-C. Pan, S.-W. Li, Y.-Y. Ho, Y.-J. Shiu, W.-L. Tsai, M. Jiao, W.-K. Lee, C.-C. Wu, C.-L. Chung, T. Chatterjee, Y.-S. Li, K.-T. Wong, H.-C. Hu, C.-C. Chen, M.-T. Lee, *Adv. Funct. Mater.* 2016, **26**, 7560.

[S9] L. Chen, Y. Jiang, H. Nie, P. Lu, H. H. Y. Sung, I. D. Williams, H. S. Kwok, F. Huang, A. Qin, Z. Zhao, B. Z. Tang, *Adv. Funct. Mater.*, 2014, **24**, 3621.

[S10] Y. Gong, J. Liu, Y. Zhang, G. He, Y. Lu, W. B. Fan, W. Z. Yuan, J. Z. Sun, Y. Zhang, *J. Mater. Chem. C.* 2014, **2**, 7552.

[S11] J. Guo, X.-L. Li, H. Nie, W. Luo, R. Hu, A. Qin, Z. Zhao, S.-J. Su, B. Z. Tang, *Chem. Mater.*, 2017, **29**, 3623.

[S12] W. Yuan, Y. Gong, S. Chen, X. Shen, J. W. Y. Lam, P. Lu, Y. Lu, Z. Wang, R. Hu, N. Xie, H. S. Kwok, Y. Zhang, J. Z. Sun, B. Z. Tang, *Chem. Mater.* 2012, **24**, 1518.

[S13] H. Li, Z. Chi, X. Zhang, B. Xu, S. Liu, Y. Zhang, J. Xu, *Chem. Commun.* 2011, **47**, 11273.

[S14] R. Furue, T. Nishimoto, I. S. Park, J. Lee, T. Yasuda, *Angew. Chem. Int. Ed.* 2016, **55**, 7171.